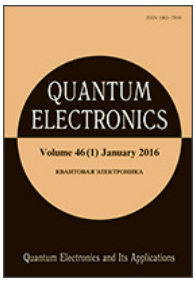

The revised version of this manuscript was published in:
V. Tosa, K. Kovács, B. Major, E. Balogh, and K. Varjú, "Propagation effects in highly ionised gas media," Quantum Electronics **46**(4), 321–326 (2016).
Available online at:
http://www.turpion.org/php/paper.phtml?journal_id=qe&paper_id=16039&year_id=2016&volume=46&issue_id=4&fpage=321&lpage=326
and
http://iopscience.iop.org/article/10.1070/QEL16039

DOI: https://doi.org/10.1070/QEL16039

Propagation effects in highly ionized gas media

V. Tosa[1,2], K. Kovács[1,2], B. Major[3], E. Balogh[3,4], K. Varjú[2,3]

[1]National Institute for R&D of Isotopic and Molecular Technologies, Cluj-Napoca, Romania

[2] ELI-HU Non-profit Ltd., Szeged, Hungary

[3] Department of Optics and Quantum Electronics, University of Szeged, Szeged, Hungary

[4] Center for Relativistic Laser Science, Institute for Basic Science (IBS), Gwangju, Republic of Korea

Introduction

The propagation of intense laser pulses in ionizing media is important in a wide range of fields, including laser-driven accelerators [1], laser-plasma channeling [2], harmonic generation [3], supercontinuum generation [4], X-ray lasers, and laser-fusion schemes (see [1] for a review).

An intense laser pulse propagating in a neutral gas is affected by diffraction, refraction, and nonlinear effects like self-focusing or self-phase modulation (SPM), ionization, and plasma defocusing [5-7]. As the beam focuses, the increased intensity results in ionization of the medium and plasma formation, hence both linear and nonlinear effects of propagation will be altered. The propagation of the bullet of light in an ionizing medium proved to be a highly non-homogeneous process both in time and in space. In time the leading part of the pulse will propagate in a neutral gas, being affected only by diffraction and neutral dispersion. As intensity increases in the pulse, the following part will be suffering from nonlinear effects (like SPM) governed by the nonlinear refractive index (n_2) of neutrals. Furthermore, for the high power laser pulses ionization starts already on the leading edge of the pulse, and following parts of the pulse will propagate through ionized medium, ionization rate depending strongly on time, so both linear and nonlinear parameters of the medium will become time-dependent. The trailing edge of

the pulse will be influenced by effects of the ionized medium, in certain cases defocusing in some cases refocusing is observed. The degree of the above modifications will be varying in radial direction which will produce complex time-space coupling during pulse propagation. When an ultrashort, intense laser pulse is used in particle acceleration experiments spatial and energy distributions of energetic electrons are shown [8,9] to depend strongly on the contrast ratio and shape of the laser prepulse. However this implies that it is essential to estimate the modifications of the shape of the pulse as induced during propagation. Moreover, the distortions induced in the temporal and spatial pedestal of an ultraintense pulse are important in these experiments and should be quantified both for characterizing the pulse and for estimating the electron concentration map to be used further in PIC simulations [10].

An active field where the propagation of an intense pulse plays an essential role is generation of high order harmonics and attosecond pulses, either single or in trains. High harmonic generation is a very perspective method for transforming the properties of infrared laser pulses to the XUV or soft-X-ray regime, thus providing unique ultrashort coherent pulses with high photon energies. Unfortunately, the conversion efficiency on the single atom level is rather weak, so harmonic radiation from many atoms has to be added constructively in order to achieve the flux level necessary in pump-probe experiments. The rapidly increasing laser pulse powers give promise to the generation of HHG in increasing magnitude, if macroscopic conditions can be chosen suitably. One option for scaling up HHG is a geometrical enlargement [11,126], keeping the system in the low ionization regime. With the peak powers promised to become available in the new laser facilities (ELI, CALA, EXCELS) this method will soon become unpractical due to the required focusing of tens-to-hundred meters. An alternative method for utilizing these high power laser pulses is in highly ionized arrangements, where phase matching is achieved in a high

density, short gas target. The two alternatives require different focusing arrangements and different gas targets, and direct experimental comparison is not available in any of the existing laboratories, let alone in the new infrastructures under development. Thus a theoretical/simulation experiment is our only means to compare the properties of the high harmonic radiation produced in the low ionization or in the high ionization arrangement.

Recently efficient soft x-ray high-harmonic generation in multiply ionized plasmas [13] was reported. Using intense UV driving lasers at 270 nm, emission in the soft x-ray domain was obtained and is assumed to be generated by ions, from Ar^{+} to Ar^{5+} ions. The authors emphasize the necessity to model pulse propagation in these media of multiple ionized atoms as well as to model harmonic generation in these conditions.

In this paper we use a three dimensional non-adiabatic model to characterize ultrashort pulse propagation in a gas medium under conditions of high intensities which creates high electron concentrations via multiple ionizations of the target atom. Although non-sequential multiple ionization is reported to occur [14] in noble gases, the dominant mechanism is sequential ionization so to calculate electron concentration we adopt a scheme that relies on rates of successive single-electron ionization events [15]. Models for pulse propagation in gas or condensed media are reviewed in [16] including numerical modeling of ultrashort pulse propagation in extreme nonlinear regimes.

Model

Propagation of an ultrashort pulse in an ionizing gas medium can be described in cylindrical coordinates by the equation [17]:

$$\nabla^2 E_1(r,z,t) - \frac{1}{c^2}\frac{\partial^2 E_1(r,z,t)}{\partial t^2} = \frac{\omega^2}{c^2}(1-\eta_{eff}^2)E_1(r,z,t) \qquad (1)$$

Where c is the speed of light, E_1 is the full electric field (carrier) with central frequency ω, and the effective refractive index is written as

$$\eta_{eff}(n_a, n_e, r, z, t) = \eta_0(n_a) + \eta_2(n_0)E_1^2(r,z,t) - \frac{\omega_p^2(n_e, r, z, t)}{2\omega^2} \tag{2}$$

and accounts for the dispersion by neutrals and electron plasma (first and respectively last term of Eq. 2) as well as for the nonlinear refractive index associated with the bound electrons (second term in Eq. 2). The last term of Eq. 2 contains the square of the plasma frequency ω_p which is proportional to the electron concentration n_e.

To solve Eq.1 it is advantageous to write it in a moving coordinate frame ($z' = z$ and $t' = t - z/c$). In the following we drop the prime symbol for simplicity, so the equation becomes:

$$\nabla^2 E_1(r,z,t) - \frac{1}{c^2}\frac{\partial^2 E_1(r,z,t)}{\partial z \partial t} = \frac{\omega^2}{c^2}(1-\eta_{eff}^2)E_1(r,z,t) \tag{3}$$

The time derivative can be eliminated by applying the Fourier transform. Also expanding the Laplace operator the equation becomes:

$$\left(\frac{\partial^2}{\partial r^2} + \frac{1}{r}\frac{\partial}{\partial r} + \frac{\partial^2}{\partial z^2}\right)E_1(r,z,\omega) - \frac{2i\omega}{c^2}\frac{\partial E_1(r,z,\omega)}{\partial z} = \frac{\omega^2}{c^2}\hat{F}\left[(1-\eta_{eff}^2)E_1(r,z,t)\right] \tag{4}$$

where $\hat{F}$ denotes the Fourier transform operator. In paraxial approximation the second derivative wrt z is neglected; therefore, the final equation to be solved numerically is:

$$\left(\frac{\partial^2}{\partial r^2} + \frac{1}{r}\frac{\partial}{\partial r}\right)E_1(r,z,\omega) - \frac{2i\omega}{c^2}\frac{\partial E_1(r,z,\omega)}{\partial z} = \frac{\omega^2}{c^2}\hat{F}\left[(1-\eta_{eff}^2)E_1(r,z,t)\right] \tag{5}$$

To solve Eq.5 numerically we use a Crank-Nicolson method written for a nonlinear scale in radial direction. The Crank-Nicolson method ensures sufficient accuracy in dealing with finite differences while the nonlinear scale allows a sufficiently large integration domain in order to avoid unphysical reflections of the propagated field on the domain walls. The right-hand side in

Eq. 5 has both an explicit dependence of the solution and an implicit one through the plasma term and Kerr term. For this reason we followed an iterative self-consistent procedure at each step of integration, as follows: after integrating over a *dz* step we obtain the propagated field E_1 in frequency domain then we use the inverse FT to obtain E_1 in time domain and recalculate the free term in Eq. 5. We then repeat the integration in frequency domain with the new source term and proceed like this until the difference between two successive laser fields is below a given threshold. Usually three to five iterations are enough, but this depends on many parameters like the number of steps in *z* direction, the initial gas pressure, initial intensity, etc.

The imaginary part of the refractive index was also considered in order to estimate the damping of the wave during propagation. We assume that the energy lost by the pulse is solely due to having to supply energy for ionization. To find this contribution we extended to multiple ionization case the method described in [18] for single ionization. In short we write the energy balance for the ionization process and assume that the energy lost by the pulse between *z* and *z+dz* is the opposite of the energy gained by the electrons in the same interval. The energy loss was estimated for each (*r*,*z*) point after every successful integration step, and the dumped field was used in the next integration step.

To integrate Eq. 5 in realistic conditions an essential ingredient is the ionization model used to calculate the ionization rates. One possible way to proceed for molecules and atoms, also adopted for the present results, is to use the Ammosov-Delone-Krainov (ADK) [19] model or its molecular version [20].

As one can see from Eq. 2 we need to estimate the electron concentration in the medium, which, in a low intensity field (10^{14} W/cm^2), originates from single (usually multiphoton or tunnel) ionization of atoms/molecules. In a very intense laser field an atom/molecule experience multiple

stripping of electrons, starting from the outer shell ones. To calculate the electron concentration we considered only sequential ionizations and developed a system of rate equations which allows the calculation of fractions of ionic species assuming the following known quantities: n_0 – initial density of the medium, $w_{01}(t)$, $w_{12}(t)$, … - ionization rates; index pairs *(k-1)k* mean ionization rate from the *(k-1)*-times ionized species to *k*-times ionized ones; rates were calculated using the ADK [19] approximation. The unknowns are $n_0(t)$, $n_1(t)$, .., $n_k(t)$ – fraction of neutrals, singly ionized, …, *k*-times ionized species.

The following system of differential equation was written and solved:

$$\frac{dn_0(t)}{dt} = -n_0(t) \cdot w_{01}(t)$$

$$\frac{dn_1(t)}{dt} = n_0(t) \cdot w_{01}(t) - n_1(t) \cdot w_{12}(t)$$

$$\vdots$$

$$\frac{dn_Z(t)}{dt} = n_{Z-1}(t) \cdot w_{(Z-1)Z}(t)$$

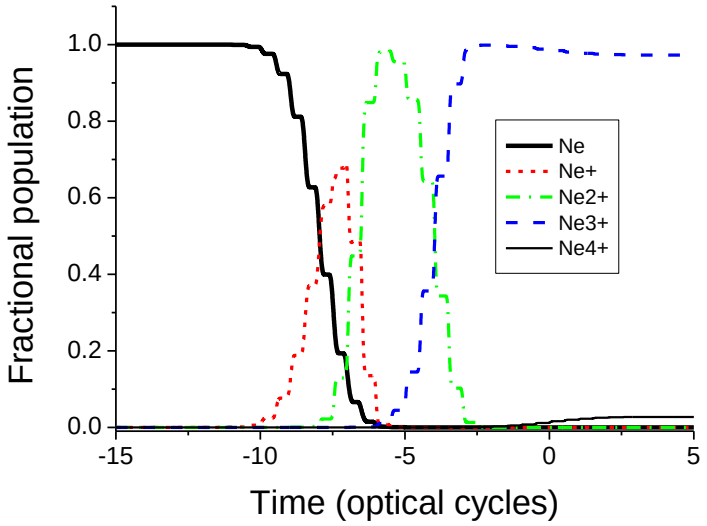

Fig.1 Temporal evolution of the ionized species starting from neutral Ne, for a peak intensity of 1.8×10^{16} W/cm^2. One can see that even Ne^{4+} still ionize and different species appears in different time ranges within the pulse.

In order to correctly evaluate the variation of the effective refractive index due to the plasma contribution, we calculate the total number of electrons resulting from this consecutive stripping of an atom/molecule:

$$n_e(t) = \sum_{k=1}^{Z} k \cdot n_k(t)$$

One brief mention should be done for the optical Kerr term in Eq. 2. As multiple ionized species are present one have to account for their contribution to the third order susceptibility χ_3 of the medium. The values of the susceptibilities for ionized atoms are not known but can be estimated. Here we used the relationship that can be established [21] between the susceptibility of the ion χ_3^+ and the susceptibility of the neutral atom χ_3^0 , their ratio being in connection with the ratio of their ionization potentials as $\chi_3^+/\chi_3^0 \approx \left(I_p^0/I_p^+\right)^3$, where I_p stands for the ionization potentials of the species involved.

Results and discussion

In the following we will focus our discussion on the case of an 800 nm femtosecond pulse propagation in Ne at 85 torr, assumed constant along a 5 mm long static cell placed in the focus. Other parameters of the calculation are as follows: pulse energy 40 mJ, pulse duration 26 fs, focal length 4 m, beam waist at the focusing element 15 mm, and we first assume an undistorted temporal pulse shape. With these conditions the waist in the focus is 68 μm and the initial intensity at medium entrance reaches the value of 1.8×10^{16} W/cm^2. Fig. 1 plots the evolution in time of ionizing species Ne, Ne^+, Ne^{2+} and Ne^{3+}. We see that Ne, and Ne^+ are fully depleted by

the end of the pulse, while Ne^{3+} and Ne^{4+} share the initial population between them. It is clear that for higher intensities one will have to consider higher and higher ionized species. If initial Ne density is assumed to be n_0 then the final electron concentration will be > $3n_0$**.** This is seen in Fig. 2 where the electron concentration and laser envelope are plotted against time. As one can note the electron concentration exhibit three plateaus, one around $-6T_0$ (corresponding to double ionization), a second around $-4T_0$ (corresponding to triple ionization) and a third one after peak maximum, related to the time evolution of the ionizing species, as seen in Fig. 1. This temporal variation of the electron concentration is highly non-homogeneous in space thus one can foresee a complex spatio-temporal variation of the refractive index which will cause interesting effects during propagation as we will see in the following.

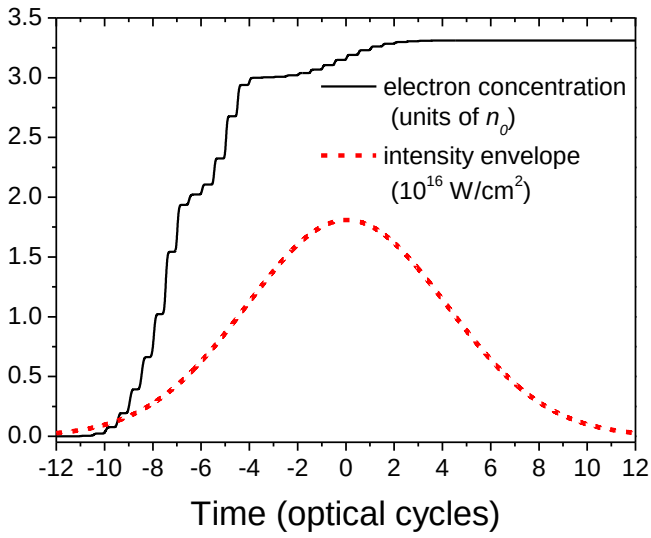

Fig. 2 Intensity envelope and electron concentration as a function of time. The time evolution of the electron concentration is connected to the evolution of the ionizing species (cf. Fig.1.).

Plotted in Fig. 3 is the spatial map of the peak intensity of the laser pulse, propagating in the ionized Ne medium, in the grid points of the interaction region. Two main features are worth to

be emphasized: the first one is the strong defocusing of the field during propagation, as electron distribution along radial direction act as a diverging lens across the beam. The second one is the pulse refocusing on axis, after ~1.5 mm of propagation. Analysis of the field in detail shows that this is due to the refractive index variation in time. In the leading part of the pulse the variation is given mainly by the electron density variation, however, when electron density comes to a stationary value the main variation of the refractive index is given by the Kerr term. This acts as a converging lens and induces a focusing of the pulse in the trailing edge, after the pulse center. One can also observe that in the peripheral regions (r>250 microns) and after z=4 mm of propagation we could not avoid a numerical boundary reflections on the domain walls, but they are weak and do not influence the values of the field in the central part. Probably for longer propagation distances these reflections become important and should be accounted for and eliminated.

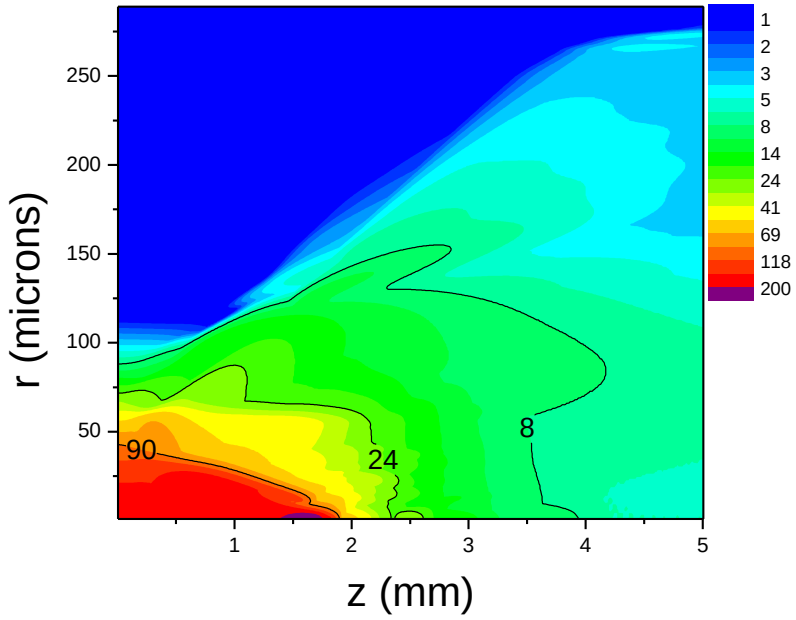

Fig. 3 Spatial map of the pulse peak intensity, in units of 10^{14} W/cm^2. An effect of boundary reflection can be seen around z=4.5 mm and r>250 microns.

It is also interesting to analyze the electron concentration in the integration domain, seen in Fig. 4. One can see the level of ionization which indicates that even Ne^{3+} is ionized. Also, the plateaus which are seen in time in Fig. 2 are present also here in space, which is another indication that there is a strong space-time coupling during pulse propagation in high ionizing conditions.

The spectral/temporal distortions which the pulse suffers during propagation in the ionizing medium will be inherited in all interactions of the laser field with matter. It is therefore essential to characterize these distortions in temporal, spectral and spatial domains, as they could be important even at optical cycle level.

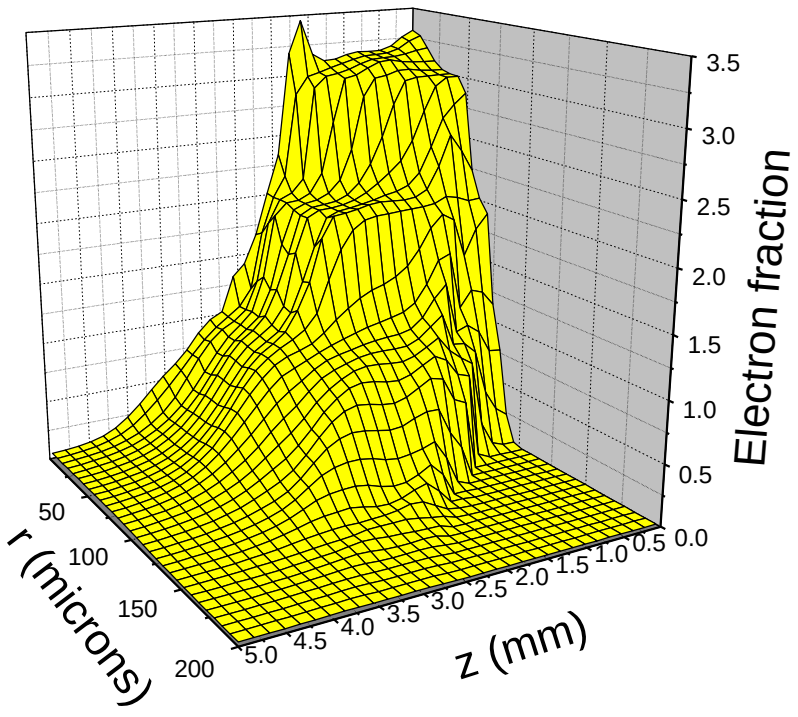

Fig. 4 Electron fraction map in units of initial neutral concentration.

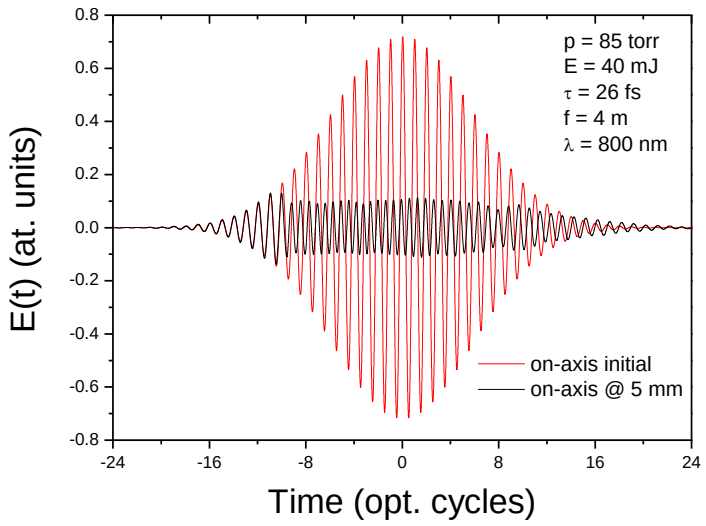

Fig. 5 Laser pulse on-axis both at medium entrance (red) and at medium exit (black)

The model we use allows this characterization because the result of the calculation is the full electric field $E_1(r,z,t)$ or its spectral counterpart $E_1(r,z,\omega)$. We show in Fig. 5 the field in time, on-axis, both at medium entrance and medium exit. As we see, the pulse experienced heavy changes in both amplitude (due to plasma defocusing) and phase (due to the time variation of the refractive index). An exception is the pulse leading part which did not produce ionization and is only slightly changed by dispersion of neutrals.

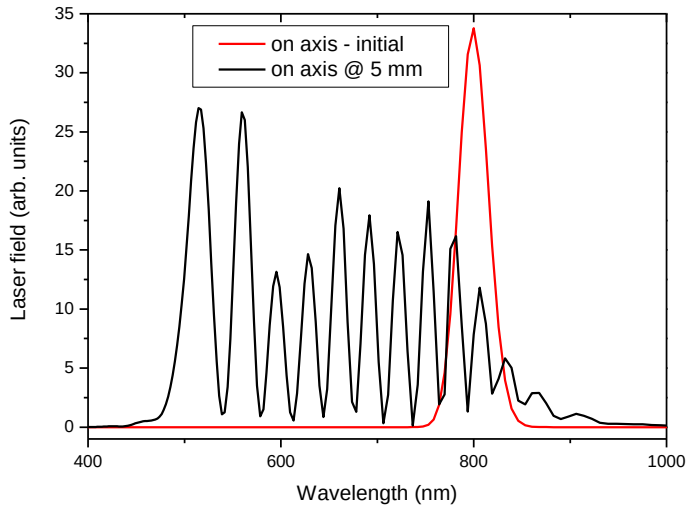

Fig. 6 Pulse spectrum at medium entrance (red) and exit (black)

Strong modifications can be seen also in frequency domain, as shown in Fig. 6. Initial spectrum is a Gaussian centered at 800 nm, while the spectrum at medium exit on-axis is heavily broadened, both towards longer but especially toward shorter wavelengths. This broadening is the effect of plasma induced self-phase modulation, similar to Kerr induced self-phase modulation. The range of broadening is noticeable, from an initial bandwidth of 50 nm centered around 800 nm (transform limited pulse), the pulse extends in a spectral domain from 470 to 950 nm after propagation.

In the case of high order harmonics generation the temporal variations of the optical parameters of the medium gives rise to macroscopic phase-matching effects that can, among others, limit the time window of effective high harmonic generation [22].

In the high intensity regime present at the first part of the gas medium, high-order harmonics can be generated both from neutrals (at the leading edge of the pulse) and from ions (after neutrals are ionized). However, in our case the high electron density prevents phase-matching of harmonics generated from ions. In fact, in this regime the main contribution to phase-mismatch comes from the plasma refractive index. However, the high-intensity regime can be explored by using UV generating fields, in which case the plasma dispersion is significantly decreased and the linear and non-linear refractive indices of ions are much larger, and cannot be neglected anymore, as was recently demonstrated in [13].

With near-infrared generating fields, phase-matched harmonic generation is mainly restricted to moderate ionization rates. The strong spatial and temporal distortions of the generating field can create conditions of efficient harmonic generation after a significant propagations length, i.e. after which the nonlinear effects diffracted the laser beam to a wider area in the gas cell, and a

homogenous intensity-distribution is achieved. This effect can be nicely seen in Fig. 7 where the map of the peak intensity over the interaction region is plotted. After propagating for about 3 mm the field stabilizes to a configuration with a constant intensity and phase over a large region in radial direction. It is interesting to note that stabilization starts from peripheral regions towards on-axis.

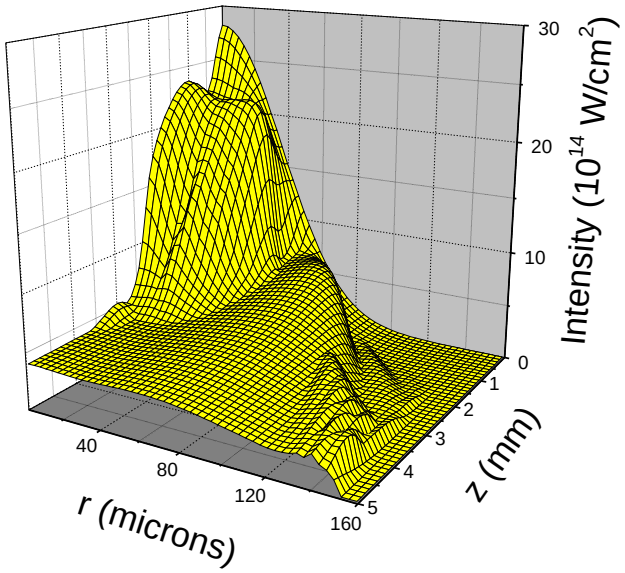

Fig. 7 Spatial map of the pulse peak intensity, in units of 10^{14} W/cm^2. After an initial strong variation in both radial and axial directions the field stabilizes over a large interaction region, favourable for harmonic generation.

The space-time coupling can also generate field configurations which give rise to unique effects in the interaction between light and matter. One example is the generation of single attosecond pulses in a lighthouse configuration, which was reported in [23]. In this case it was demonstrated numerically that a multicycle laser pulse (800 nm, 25 fs) gains, in conditions of high ionizations, a rotating wavefront which, generating high order harmonics in interaction with Ar atoms,

produce single attosecond pulses in successive half-cycles and with increasing divergence. The overall effect is a series of single attosecond pulses emitted in conical shapes of increasing angles, from one half-cycle to the next half-cycle.

Conclusions

Solving the case of an ultra-intense pulse propagating in gaseous media is performed via a non-adiabatic three dimensional model which was extended to the case of multi-ionization for the atomic species present in the interaction region. The results demonstrate a complex space-time coupling during pulse propagation and strong temporal/spectral modifications of the pulse. The field configuration can, in specific conditions, generate interesting effects, attosecond lighthouse emission being demonstrated for the case of Ar.

Acknowledgements

V.T. and K.K. gratefully acknowledge financial support from projects RO-CERN E02 (PULSE-PROPAG) and PN-II-ID-PCE-2012-4-0342.

References

1. E. Esarey, C. B. Schroeder, and W. P. Leemans, Rev. Mod. Phys. **81**, 1229, (2009)
2. Min Chen, Ji Luo, Fei-Yu Li, Feng Liu, Zheng-Ming Sheng, Jie Zhang, Light: Science & Applications **5**, e16015 (2016)
3. F.Krausz, M. Ivanov, Rev. Mod. Phys. **81**, 163-234 (2009)
4. E. E Serebryannikov, E. Goulielmakis, A. M. Zheltikov, New Journal of Physics **10**, 093001 (2008)
5. E.S. Efimenko, A.V. Kim, and M.Quiroga-Teixeiro, Phys.Plasmas, **18**, 032107 (2011).
6. S. C. Rae and K. Burnett, Phys. Rev. A **46**, 1084 (1992)
7. S. C. Rae, Optics Communications **104**, 330 (1993)
8. T. Hosokai, K. Kinoshita, A. Zhidkov, K. Nakamura, T. Watanabe, T. Ueda, H. Kotaki, M. Kando, K. Nakajima, and M. Uesaka, Phys. Rev. E **67**, 036407(2003).
9. H. T. Kim, K. H. Pae, H. J. Cha, I. J. Kim, T. J. Yu, J. H. Sung, S. K. Lee, T. M. Jeong, and J. Lee, Phys. Rev. Lett. **111**, 165002(2013).
10. Hyung Taek Kim, Ki Hong Pae, Hyuk Jin Cha, I Jong Kim, Tae Jun Yu, Jae Hee Sung, Seong Ku Lee, Tae Moon Jeong, and Jongmin Lee, Phys. Rev. Lett. **111**, 165002 (2013)

11. P. Rudawski, C. M. Heyl, F. Brizuela, J. Schwenke, A. Persson, E. Mansten, R. Rakowski, L. Rading, F. Campi, B. Kim, P. Johnsson, A. L. Huillier, P. Rudawski, C. M. Heyl, F. Brizuela, J. Schwenke, A. Persson, and E. Mansten, Rev. Sci. Instrum. **84**, 073103 (2013).
12. C. M. Heyl, H. Coudert-Alteirac, M. Miranda, M. Louisy, K. Kovacs, V. Tosa, E. Balogh, K. Varjú, A. L'Huillier, A. Couairon, and C. L. Arnold, Optica, **3**, 75 (2016)
13. D. Popmintchev, F. Dollar, C. Mancuso, M. Chen, A. Hankla, X. Gao, B. Shim, A. L. Gaeta, M. Tarazkar, D. A. Romanov, R. J. Levis, J. A. Gaffney, M. Foord, S. B. Libby, A. Jaron-Becker, A. Becker, L. Plaja, M. M. Murnane, H. C. Kapteyn, and T. Popmintchev, Science **350**, 1225 (2015).
14. S. Larochelle, A. Talebpour, and S. L. Chin, J. Phys. B At. Mol. Opt. Phys. **31**, 1201 (1999);
15. P. G. A. Martínez and L. Bergé, J. Phys. B At. Mol. Opt. Phys. **47**, 204017 (12pp) (2014); P. G. A. Martínez, A. C. La Fontaine, C. Köhler, and L. Bergé, J. Phys. B At. Mol. Opt. Phys. **48**, 094010 (2015).
16. M. Kolesik and J. V Moloney, Rep. Prog. Phys. **77**, 016401 (2014); A. Couairon, E. Brambilla, T. Corti, D. Majus, and M. Kolesik, Eur. Phys. J Spec. Top. **199**, 5 (2011).
17. V. Tosa, K. T. Kim, and C. H. Nam, Phys. Rev. A **79**, 043828 (2009)
18. E. Takahashi, V. Tosa, Y. Nabekawa, K. Midorikawa, Phys. Rev. A **68**, 023808 (2003)
19. M.V. Ammosov, N.B. Delone, V.P. Krainov, Sov. Phys. JETP **64**, 1191 (1986)
20. X.M. Tong, Z.X. Zhao, and C.D. Lin, Phys. Rev A, 66, 033402 (2002)
21. P. Sprangle, E. Esarey, and B. Hafizi, Phys. Rev. Lett. **79**, 1049 (1997).
22. B. Schutte, P. Weber, K. Kovacs, E. Balogh, B. Major, V. Tosa, S. Han, M. J. J. Vrakking, K. Varju, and A. Rouzee, Optics Express **23**, 33947 (2015)
23. V. Tosa, J. S. Lee, H. T. Kim, and C. H. Nam, Phys. Rev. A, **91**, 051801(R) (2015)